EXTENSIONAL FALL OF A VERY VISCOUS FLUID DROP

by Y. M. STOKES, E. O. TUCK

(*Department of Applied Mathematics, The University of Adelaide, South Australia 5005, Australia*)

and L. W. SCHWARTZ

(*The University of Delaware, USA*)

[Received 25 January 1999. Revise 6 January 2000]

Summary

A finite drop of fluid with large viscosity μ and density ρ is initially at rest hanging under gravity g from the underside of a solid boundary. The initial configuration may be of a general boundary shape, with (vertical) maximum length $L(0) = L_0$ and (horizontal) maximum width w_0. The subsequent motion, drop length $L(t)$ as a function of time t, and boundary shape is determined both by a slender-drop approximate theory (for $w_0 \ll L_0$) and by an exact finite-element calculation. The slender-drop theory is derived both by Lagrangian and Eulerian methods. A wall boundary layer is identified, and empirical corrections made to the Trouton viscosity appearing in the slender-drop theory to account for this layer. When inertia is neglected, there is a crisis at a finite time $t = t_* = O(\mu/(\rho g L_0))$, such that $L(t) \to \infty$ as $t \to t_*$, this time being related to the time of break-off and entry of the drop into free fall. When the break point falls outside the wall boundary layer, its location and hence the fraction of the original drop which falls can be obtained directly from the slender-drop theory, and is confirmed by the finite-element computations.

1. Introduction

An inverted spoonful of honey may appear to take several seconds to begin to move, but then at an ever-increasing rate it forms itself into a drop, which falls quickly under gravity. If its consistency is smooth, and no barrier intrudes, the honey drop will fall almost freely, though remaining connected to the spoon by a very fine and long continually-extending filament. Figure 1 shows some frames from a simulation of this flow, computed using a finite-element program to be discussed later; the full MPEG movie is available on the Web; see (**1**).

The events so described and illustrated occur in a finite time. That time is essentially independent of how far the drop is allowed to fall, the final free-fall time being very short compared to the time during which viscous forces dominate while the drop is being formed. We shall refer to this as the *finite-time phenomenon*, and to the time at which fall occurs as the *crisis time*.

Dripping honey (**2**) is just one commonly observed example of a class of motions which can be described as extensional flows (**3**, **4**). Others include spinning and drawing of polymer or glass fibres for use in textiles, glass reinforced plastics, or optical fibres (**5**, **6**, **7**), and web spinning by spiders and insects; continuous drawing of sheet glass (**7**); glass-blowing and blow-moulding in the manufacture of containers, light bulbs, and glass tubing (**7**, **8**); rheological measurement by fibre extension and fibre spinning for polymers and glasses (**9**, **10**); and in geophysics examples in the areas of oil recovery (see (**11**)) and flows beneath the earth's crust that possibly lead to mountain formation and volcanic activity (**12**, **13**, **14**). Not all of the above applications exhibit the finite-time phenomenon described for the honey drop, and even in cases where it is very likely to occur, it is

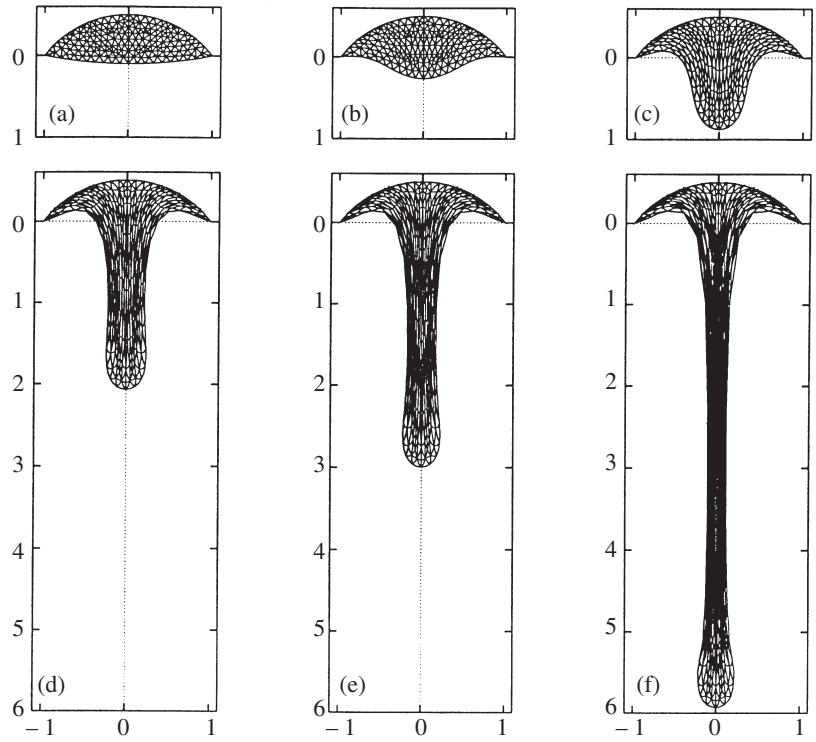

Fig. 1 Sequence in the fall of an axisymmetric honey drop from a spherical-cap spoon. (a) $t = 0$, (b) $t = 20$, (c) $t = 35$, (d) $t = 40$, (e) $t = 41$, (f) $t = 42$

not always observed, perhaps because the flow is heavily modified in the extreme end stages of the processes being considered.

There is a considerable amount of literature concerning the breaking of liquid jets/filaments to form drops. Liquids ranging from very viscous through to essentially inviscid have been studied. Most of this work has focused on drop formation when the jet radius goes to zero in a finite time as a result of surface tension; see for example (**15**, **16**, **17**). In these papers, extension under gravity is not an issue, which it certainly is for the case of dripping honey.

Gravity-driven slow dripping of a viscous fluid emerging from a narrow vertical tube has been considered by Wilson (**18**), both with and without surface tension effects, with particular attention being given to the mass of the drops that form and break away. The flow is modelled by a one-dimensional slender-drop theory utilizing conservation of mass, force balance on fluid particles, and the Trouton approximation (**3**, **4**, **19**) relating stress and rate of strain for extensional flows. A finite-time phenomenon and crisis time is identified, similar to that for dripping honey, even with surface tension neglected, when the cross-sectional area of the drop at some point becomes zero so that it breaks. Because of the neglect of inertia, the model also indicates that the drop length becomes infinite at this crisis time. Wilson notes that this physical impossibility can be removed by including inertia in the equations; then (subsequent to a rapid increase near the crisis time) the drop length will (relatively slowly) tend to infinity and the cross-sectional area will tend to zero as time

goes to infinity, with the ultimate break-off of the drop being caused by mechanisms of instability. These mechanisms, however, become important only at times very close to the crisis time, and hence an inertia-less model that predicts a finite crisis time is suitable for determining drop volume and an estimate of the actual time of rupture.

Gravity-driven extensional flow has also been considered in a geophysical context by Canright (**12**) and Houseman and Molnar (**14**). Analysis of the stability of a very viscous fluid layer overlying a less dense and much less viscous fluid shows that, when perturbed, vertical 'fingers' of the very viscous fluid grow and extend under gravity into the lower less dense fluid. With neglect of inertia, these fingers become infinite in length in a finite time. This type of flow may be a mechanism in the formation of mountains, as 'drops' of the Earth's lithosphere descend into the asthenosphere (**14**), and could conceivably cause other catastrophic geological events.

Fibre spinning is well discussed in the literature (for example, (**5**, **20**)). Typically, in the manufacturing process, the molten fibre material leaving the spinnerette rapidly solidifies and is taken up on a winder. Because the fibre is pulled at a constant rate, and because of the solidifying of the fluid, a true finite-time phenomenon cannot occur (**6**). Schultz and Davis (**20**) also consider a fibre stretching under its own weight, and, although it was not discussed in that paper, this is an example where the finite-time phenomenon will occur provided solidification does not happen too quickly. The finite-time phenomenon for a one-dimensional viscous fibre stretching under gravity and/or an applied force is mentioned by Kaye (**21**).

Drawing of viscous sheets, as in the manufacture of sheet glass (**7**), is quite similar to fibre spinning, and has been modelled by Howell (**22**) using a thin-sheet approximation to the Stokes equations. Again, a constant drawing velocity and solidification preclude any finite-time phenomenon.

The 'liquid bridge' (**11**) is a simplified extensional-flow model that is widely used for flows such as have been mentioned above. A cylindrical column of fluid attached at its ends to two coaxial discs of equal radius is stretched by pulling the discs apart. When the discs are pulled apart with a constant velocity (**11**) or with a velocity that increases exponentially in time (**10**), the finite-time phenomenon will not occur, since it will take an infinite time for the liquid bridge to reach infinite length (ignoring other factors such as surface tension that cause it to break) (**6**). If, on the other hand, stretching is caused by gravity, say by attaching a falling weight to one disc (**9**), then the finite-time phenomenon will occur. Much attention has been paid to the mechanisms causing breaking of a liquid bridge and the influence of surface tension, gravity and other factors (**11**). As for the slowly-dripping fluid discussed previously, it is likely that, for the types of extensional flow we are considering where the finite-time phenomenon is a feature, these factors become important mainly at or close to the crisis time.

A different extensional flow to those we have mentioned so far is pressure-driven flow of high-viscosity thin films such as is used in glass-blowing and blow-moulding (**7**, **8**, **23**). Stretching of a molten viscous material such as glass or polymer results from applying a pressure difference across the thickness of the film to cause substantial motion in this transverse direction. Where there is no mould interference, the finite-time phenomenon is a feature of this flow, with the radius of the arc formed by the sheet becoming infinite in a finite time (**24**).

In the present paper, we solve for the time-dependent motion, shape and length of a finite mass of Newtonian fluid of large constant viscosity that is initially at rest beneath and in contact with a solid boundary.

The most straightforward procedure for solving this problem is to use standard computational fluid-dynamic tools such as the finite-element method (**25**) to solve the three-dimensional equations

of motion, subject to no-slip boundary conditions on the solid boundary and zero-stress conditions on the free surface. In this way we can study drops of arbitrary initial shape. The finite-element method is the preferred method for numerically modelling a variety of forming processes (**23**, **26**). It has been used to simulate liquid bridges (**27**), although the use there of a mesh with fixed axial length requires that the simulation be restricted to low-rate and small-deformation experiments. In our dripping-honey example, once the drop begins to move, it quickly elongates in the direction of gravity. In order to cope with these large elongations, we employ a finite-element method with a moving mesh, such as has been applied to the modelling of blow moulding of containers (**28**, **29**, **30**), the growth of 'fingers' in the Earth's lithosphere (**14**), and by the present authors to slumping under gravity of molten glass in the form of a bridge (**31**) or a lens (**32**, **33**).

However, because of the large elongations seen in the types of flow we are considering, a slenderness assumption is also possible once this elongation has occurred, leading to an approximate one-dimensional theory, cf. (**6**, **20**, **21**). This slenderness assumption may also be valid initially, and we assume in constructing the approximation that our interest in the flow begins at a time when this is so. The resulting one-dimensional flow can be described either by Lagrangian or Eulerian methods, and we demonstrate equivalence between these two viewpoints here. Comparison with the exact finite-element computations helps to clarify the regime where the slender-drop theory is valid.

Our solutions are obtained with neglect of inertia, on the basis that the viscosity is large, strictly that an appropriate Reynolds number is small; the flow is thus creeping or Stokes flow and requires accelerations that are very small compared to the acceleration of gravity. The most important theoretical conclusion from these solutions is that the drop length eventually increases rapidly, and appears to become infinite at a finite crisis time. This was noted by Wilson (**18**) and Canright (**12**), and is an inevitable and explicit property of the approximate slender-drop theory used by these authors and in the present paper. It is also confirmed numerically by the present exact finite-element computations. The latter computations must eventually fail when the computational grid becomes unreasonably stretched and the velocities very large. Nevertheless, when applied to drops that are initially sufficiently slender, they predict drop lengths that are increasing extremely rapidly near to finite crisis times that are in close agreement with those predicted by the approximate theory.

In the real world, drop lengths cannot of course become infinite, although the honey example shows that the overall length of the drop plus its connecting filament can indeed become very large compared to the initial drop length. Meanwhile, however, the main falling head of the drop develops an acceleration comparable to that of gravity, as the remaining ever-thinning filament connection loses its ability to restrain the main drop's transition into free fall. In that phase of the motion, but only at times that are very close to the predicted crisis time, the assumption of neglect of inertia loses its validity. However, as discussed in (**18**), for fluids of large viscosity, it may be expected that the present results will provide good approximations until quite close to the crisis time, and in particular will provide a useful prediction of the actual value of the crisis or filament-breaking time and of the break point or fraction of the initial drop that falls.

2. Mathematical formulation

Suppose at any time the fluid mass lies in $0 < x < L(t)$, $|y| < f(x, z, t)$, and is an incompressible Newtonian viscous fluid of density ρ and viscosity μ, in a gravity field g acting in the x-direction. Symmetry of the drop with respect to the y-coordinate is not an essential assumption, but is used

here for simplicity. We neglect inertia and therefore have to solve the Stokes equations (**34**, p. 217)

$$p_x = \mu\nabla^2 u + \rho g, \tag{1}$$

$$p_y = \mu\nabla^2 v, \tag{2}$$

$$p_z = \mu\nabla^2 w, \tag{3}$$

and the continuity equation

$$u_x + v_y + w_z = 0, \tag{4}$$

subject to no-slip boundary conditions

$$u = v = w = 0 \tag{5}$$

at the wall, which is assumed to lie in or close to the plane $x = 0$, and no-stress free-boundary conditions (**35**, p. 452)

$$(-p/\mu + 2u_x)(-f_x) + (u_y + v_x) + (u_z + w_x)(-f_z) = 0, \tag{6}$$

$$(u_y + v_x)(-f_x) + (-p/\mu + 2v_y) + (v_z + w_y)(-f_z) = 0, \tag{7}$$

$$(u_z + w_x)(-f_x) + (v_z + w_y) + (-p/\mu + 2v_y)(-f_z) = 0, \tag{8}$$

at the side boundary $y = f(x, z, t)$. We must also satisfy a kinematic boundary condition

$$f_t = v - f_x u - f_z w \tag{9}$$

on the side boundary. If the drop has a rectangularly cut-off bottom, that is, if $f(x, z, t)$ is not zero at $x = L(t)$, similar free-boundary conditions must also be satisfied on the bottom surface.

Our task is to solve the equations (1) to (4) subject to boundary conditions (5) to (9) and suitable initial conditions. We shall do this numerically in both two and three dimensions by finite-element methods, but first discuss an approximate one-dimensional solution.

3. Slender-drop theory

It is possible to provide an approximate solution of the equations in section 2 for slender drops, that is, those drops such that the free-surface slope f_x in the vertical direction is everywhere small. The net effect of such an approximation will be that the flow is determined largely one-dimensionally, the key variables being a measure $u(x, t)$ (averaged over a cross-section at fixed x) of the downward vertical velocity, and the net cross-sectional area

$$A(x, t) = 2\int f(x, z, t)dz \tag{10}$$

of the drop at station x.

Derivation of appropriate equations to determine u and A can be done in one of two ways. The simplest way is to convert to a Lagrangian specification $x = X(\xi, t)$, in which $u = X_t$. This Lagrangian derivation was given by Wilson (**18**) and only the final equations are provided here. The label variable ξ is such that $x = \xi$ at $t = 0$. The area A is then to be determined as a function of ξ and t, subject to an initial value $A = A_0(\xi)$ at $t = 0$.

Conservation of mass combined with a 'constitutive' equation relating one-dimensional stress and rate of strain yields such a formula for A, namely

$$A(\xi, t) = A_0(\xi) - \frac{\rho g t}{\mu_*} \int_{\xi}^{L_0} A_0(\xi_1) d\xi_1, \tag{11}$$

where μ_* is the so-called 'Trouton viscosity' (**19**; **3**, p. 30) which is related to the actual viscosity μ by $\mu_* = 3\mu$ in three dimensions, and $\mu_* = 4\mu$ in two dimensions. Meanwhile, mass conservation demands that

$$X(\xi, t) = \int_0^{\xi} \frac{A_0(\xi_1)}{A(\xi_1, t)} d\xi_1. \tag{12}$$

Combination of these two equations yields via two quadratures all required information about the flow, given any specification $A_0(\xi)$ of the initial shape. In particular, if required, the velocity u can then be obtained by time differentiation, and the length $L(t)$ of the drop at any time is just given by $L(t) = X(L_0, t)$.

An alternative Eulerian derivation of these results proceeds via a formal asymptotic expansion with respect to a small parameter $\epsilon = w_0/L_0$, where $w_0/2$ is the maximum value of $f(x, z, t)$. This leads to equations for the one-dimensional dependent variables $u(x, t)$ and $A(x, t)$, namely

$$\frac{\partial}{\partial x}\left[A \frac{\partial u}{\partial x}\right] + \frac{\rho g}{\mu_*} A = 0, \tag{13}$$

involving the Trouton viscosity μ_* again, and

$$\frac{\partial A}{\partial t} + \frac{\partial}{\partial x}[uA] = 0. \tag{14}$$

Equation (13) has previously been derived (for example, (**6**, **22**)) in the absence of gravity, when its solution is immediate. With the gravity term present, the best procedure to solve (13) coupled with (14) is in fact to revert to the Lagrangian representation.

Recognizing equation (14) as a one-dimensional continuity equation, it is not difficult to make the appropriate changes of variable to retrieve the Lagrangian-representation equations above. For example, (13) integrates with respect to x to give $-Au_x$ in terms of the weight of the drop beneath coordinate x, while (14) then shows that this quantity is equal to the time derivative of A following a fluid particle; hence (11) follows by time integration.

We shall discuss the general case of the above approximate solution later, but for now let us simply observe the special case in which $A_0(x) =$ constant. This applies both in two dimensions to an initially rectangular slab, and in three dimensions to an initially cylindrical drop of a general (constant) cross-section. Then we find a length given by

$$\frac{L(t)}{L_0} = -\frac{t_*}{t} \log\left(1 - \frac{t}{t_*}\right), \tag{15}$$

where

$$t_* = \frac{\mu_*}{\rho g L_0}. \tag{16}$$

Thus it is explicit that the solution 'blows up', with $L(t) \to \infty$ at the finite crisis time $t = t_*$. It is also clear by substitution into (11) that the area at $\xi = 0$ goes to zero at this crisis time t_*, so that according to this approximation, the whole fluid mass breaks away from the wall at that time, cf. (**18**). For some other initial drop shapes, some fluid will remain attached to the wall; see later.

4. Finite-element procedure and convergence tests.

The problem as formulated in section 2 is suitable for immediate solution using the finite-element method. We have used such code (**33**) to solve these equations in two-dimensional and axisymmetric cases, although in principle the general three-dimensional equations can be solved as easily. We use 6-node triangular mesh elements with quadratic basis functions for velocity, and linear basis functions for pressure. For numerical integration over a triangular mesh element, we use a four-point quadrature rule which is exact for cubic polynomials and which employs only points interior to the element. The nominal order of convergence (**36**) of the resulting finite-element code is then $O(h^3)$, where h is a measure of mesh-element size.

To obtain the time evolution of the geometry we solve

$$\tilde{q} = d\tilde{r}/dt \tag{17}$$

for the position vector $\tilde{r} = (x, y, z)$, given the velocity vector $\tilde{q} = (u, v, w)$, at each of the mesh nodes, using a fourth-order Runge–Kutta method. The mesh nodes are then moved to their new positions (that is, they are material nodes), and this constitutes a new meshed geometry, on which the whole procedure may be repeated. This process continues until a time is reached when there is an extremely rapid distortion of the mesh, a time beyond which our computations cannot be continued. This time will be identified with the 'crisis time' predicted by the slender-drop theory.

To demonstrate convergence of our numerical methods, let us first take an initially rectangular two-dimensional slab with a width/length ratio of 0·2, attached to a plane no-slip wall $x = 0$. We use a non-dimensional formulation, with a length scale of L_0 and a time scale of $\mu_*/(\rho g L_0)$. This means that the slender-drop approximation to the crisis time for this particular initial drop shape is $t_* = 1$. We exploit the lateral symmetry of the problem to reduce our computations to half of the rectangular domain, and demonstrate convergence with respect to both mesh and time-step sizes.

Convergence with increasing numbers of mesh elements has been investigated both for uniform meshes and for non-uniform meshes with elements concentrated at the contact corners. As a first test, we evaluate the impulsively developed velocities at the initial instant of time $t = 0_+$, and examine convergence of the computed value of the maximum velocity, which occurs at $(x, y) = (0, 1)$ and is the initial rate of extension $L'(0_+)$. As in previous work (**31**), the non-uniform mesh was found to converge faster than the uniform mesh. It is also preferred because mesh elements are clustered in the area which will see most distortion as time progresses. The results for the non-uniform mesh are given in Table 1, from which we conclude that a mesh of about 150 elements (in one half of the domain) is suitable for this geometry and gives about three figures of accuracy.

With respect to convergence with decreasing time step, we consider both the drop length $L(t)$ and rate of extension dL/dt. We have found the Runge–Kutta method to give excellent accuracy at times not too close to the crisis time, even for quite large time steps. Accuracy decreases near crisis time where mesh movements are large, and is clearly identified by non-conservation of flow domain area (equivalent to non-conservation of mass). Because of this, we place a restriction on the displacement of any node in a single time step, reducing the time step if necessary to satisfy this condition. This has the effect of clustering time steps near the crisis time, when there is most action.

Table 1 Rate of extension at $t = 0$

No. of elements	dL/dt
66	0·029911
146	0·029923
235	0·029926
315	0·029925
409	0·029929
501	0·029929

Table 2 Length and rate of extension at $t = 1$

$\triangle t$	$\lvert\triangle\tilde{r}\rvert$	No. of timesteps	L	dL/dt	Area
0·25	0·50	5	3·019435	0·772955	0·2001449
0·05	0·50	20	3·017544	0·773823	0·2000013
0·25	0·10	20	3·017533	0·773826	0·2000010
0·05	0·10	27	3·017522	0·773827	0·2000001
0·25	0·05	41	3·017522	0·773829	0·2000000
0·05	0·05	43	3·017522	0·773829	0·2000000

Table 2 gives some results at $t = 1$, which is very near the crisis time for our test geometry, for different values of maximum time step $\triangle t$ and maximum permitted displacement $|\triangle\tilde{r}|$. A non-uniform mesh of 146 elements was used. In fact, $t = 1$ is the non-dimensional crisis time t_* in the slender-drop limit, and the effect of thickness is just to increase this time slightly. Considering the extreme proximity of crisis, where we expect catastrophic loss of accuracy, these results are extremely good. We have good conservation of mass (area) with six figure accuracy for $\triangle t = 0{\cdot}05$ and $|\triangle\tilde{r}| = 0{\cdot}10$. The corresponding values of L and dL/dt show convergence to seven and five figures respectively.

Obviously, we are unable to compute at exactly the crisis time, and can only hope to approach it as closely as possible. Not unexpectedly, as we approach closer to this crisis time, some of the mesh elements become very distorted due to the large elongation and pinching-in near the wall, resulting in numerical error. Re-meshing the flow domain before the elements become too distorted and too much numerical error results, enables us to compute closer to the crisis time, until again the mesh elements become excessively distorted. Eventually we reach a point where we cannot compute any further, even if we re-mesh. To obtain an estimate for the crisis time itself, we plot L^{-2} versus time t, and extrapolate to $L^{-2} = 0$.

It is instructive to further treat the case of a rectangular initial drop shape, but now with varying aspect ratio (width/length). As already indicated, there are no extra computational difficulties associated with the axisymmetric equivalent of the two-dimensional problem, namely an initially cylindrical drop, and the results are qualitatively similar. Furthermore, as previously indicated (section 3), in the slender-drop limit the two- and three-dimensional crisis times differ only by a factor of three-quarters—the ratio of Trouton viscosities. Since we consistently non-dimensionalize the finite-element computations with respect to a time scale involving the Trouton viscosity, the non-dimensional slender-body estimate of the crisis time remains at $t = 1$ in both three and two dimensions.

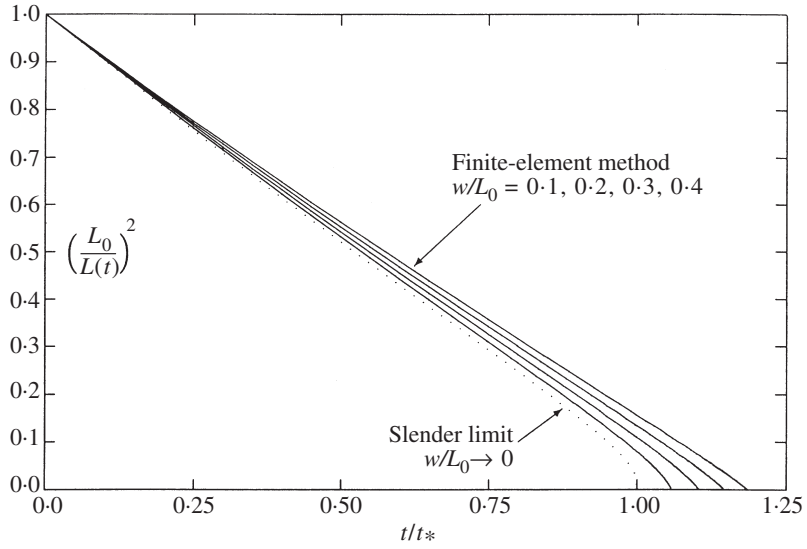

Fig. 2 Length versus time for rectangular slabs

We first consider initially-rectangular two-dimensional slabs with aspect ratios between 0·1 and 0·4, and with meshes of between 155 and 175 elements over the half-domain. Figure 2 gives finite-element computations of L^{-2} versus t for the different aspect ratios considered, and the slender-drop theory is also shown (dotted) for comparison. There is no extrapolation in this figure; the results were computed until a time close enough to the crisis for the curves to appear to reach the 'axis' $L^{-2} = 0$ of effectively infinite drop length on the scale of this figure. A particular advantage of plotting L^{-2} is that the small-time behaviour predicted by the slender-drop theory is a straight line passing exactly through the crisis point; the actual curve is then just a small upward deviation from this line. The slender-drop theory is the small-aspect-ratio limit, and the agreement between the slender-drop and finite-element computations is good for the lower aspect ratios, as expected.

Figures 3 and 4 show in parts (a) the evolution of the shape of the drop of initial aspect ratio 0·2, as given by the finite-element method, at times $t = 0{\cdot}75$ and $t = 0{\cdot}95$ respectively. The slender-drop approximate profiles are also given for comparison in parts (b) of these figures, the uncorrected profiles being the lower of the two curves in each case. There are two types of apparent difference between the exact finite-element computations and the uncorrected slender-drop theory, namely an upward shift of the profile and a modified profile near the wall. The main effect of finite width is related to this boundary layer that develops at the wall, which then affects the timescale, so that the actual drops fall slightly slower than the slender-drop theory predicts. Otherwise, the exact (finite-difference) and approximate (slender-drop) profile shapes are very close if corrected to compensate for this small time difference, except for the region near the wall which we now discuss.

5. Wall boundary layer

The slender-drop solution satisfies two boundary conditions on the velocity $u(x, t)$, corresponding to the second-order character of the partial differential equation (13). Namely $u = 0$ at $x = 0$ and $u_x = 0$ at $x = L(t)$. The first is a condition of zero normal velocity at the wall, the second

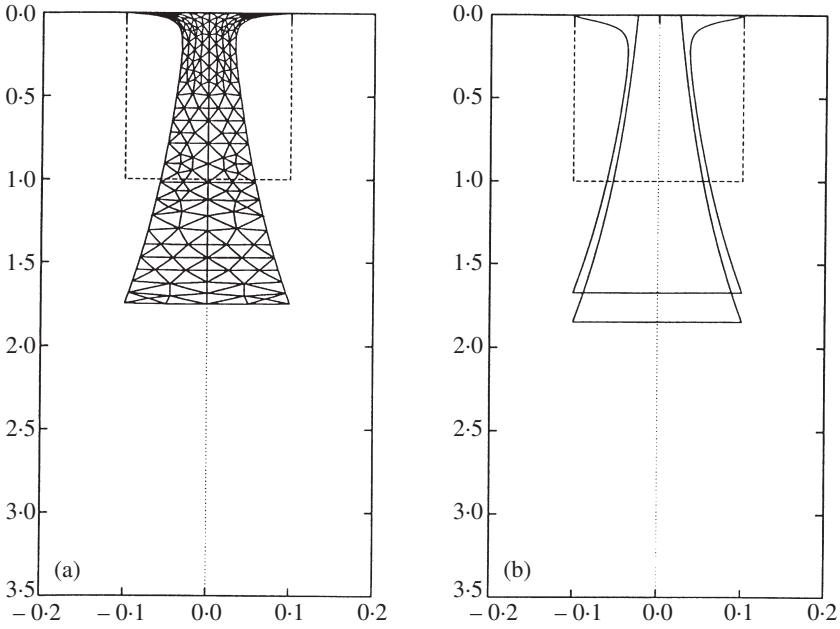

Fig. 3 Initially-rectangular profile, at $t = 0{\cdot}75$. (a) Finite-element method. (b) Slender-drop theory, with and without boundary correction

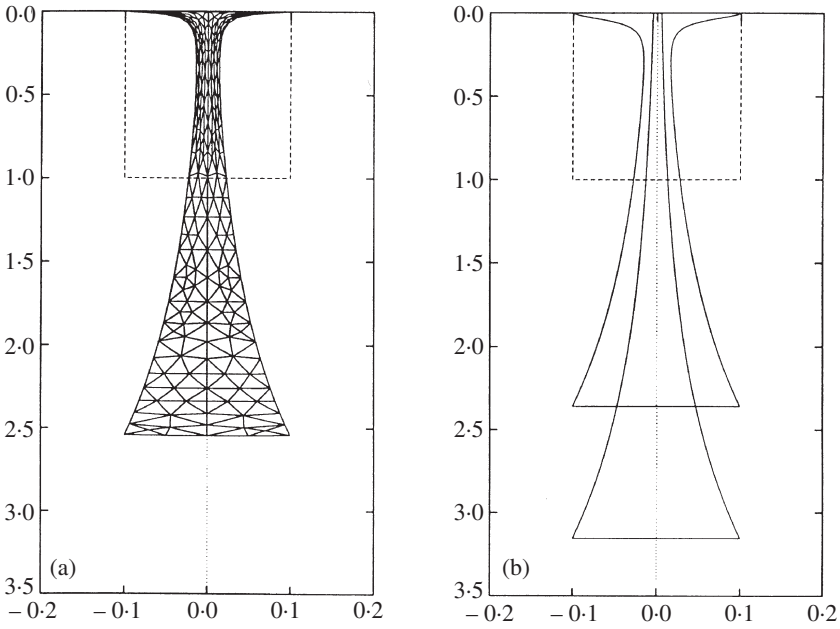

Fig. 4 Initially-rectangular profile, at $t = 0{\cdot}95$. (a) Finite-element method. (b) Slender-drop theory, with and without boundary correction

a condition of zero normal stress at the bottom. What is missing is a condition such as $u_x = 0$ at $x = 0$, which would have ensured no-slip at the wall. Hence in this sense, the slender-drop theory is an outer singular perturbation (**20**), analogous to the inviscid assumption at high Reynolds number. If we wish to describe the flow near the wall more accurately, we need to match with an inner approximation analogous to a boundary layer.

In the exact problem, the free surface of the drop remains tethered to the wall at its initial position, whereas the slender-drop theory suggests that its outer edges move inward with time, slipping along the wall. As we see from the finite-element computations, this is not an unreasonable description of the behaviour at a cross-section a short distance below the wall, that distance being of the (vertical) extent of about one drop thickness. Between the wall and that cross-section, the exact solution compensates for failure of the slender-drop theory to satisfy no-slip, and in that region the velocities are not dominated by vertical motion, and the free surfaces are not close to vertical, so that the slender-drop assumptions are not valid. The flow in this inner domain is not easy to analyse, and in one sense the finite-element computation provides the best way to do so.

However, it is possible to give an empirical discussion of the wall boundary layer, leading to a correction to the slender-drop theory, as follows. An approximate model for flow near the top no-slip boundary can be found using a variant of the 'squeeze bearing' problem (**37**, p. 392), of lubrication theory. In that problem, two parallel rigid no-slip walls, separated by a small distance, move relative to one another in the direction normal to their surfaces. A viscous liquid occupies a portion of the space between them, with the edges of the liquid region open to the atmosphere. A thin-layer momentum equation coupled with mass conservation and overall force balance in the direction normal to the plates allows the prediction of plate speed as a function of spacing, width of the liquid-filled region, liquid viscosity and the applied force. The particular modifications appropriate to the present wall boundary layer will now be described in more detail for the two-dimensional case.

As before, the liquid region is bounded above by the stationary y-axis, upon which the condition $v = 0$ is imposed. Let us assume that the extent of this boundary is $|y| < w_0/2$. A second artificial material boundary is now taken to be the line $x = h(t) > 0$, on which the stress component proportional to v_x is taken as zero. This kinematically and dynamically constrained flow is representative of the shear-dominated region when h is small. The simplified momentum equation is

$$p_y = \mu v_{xx} \tag{18}$$

and the inward flux through any station y is

$$\int_0^h v dx = -y h_t \tag{19}$$

by mass conservation. Because h is small, p_y is independent of x and the velocity profile is parabolic. Performing the flux integration and imposing the boundary condition $p = 0$ at $y = \pm w_0/2$, the pressure variation is

$$p = -\frac{3\mu h_t}{2h^3}\left[w_0^2/4 - y^2\right]. \tag{20}$$

The integral of the pressure from $-w_0/2$ to $w_0/2$ is equated to the tension or weight $-W$. This

equality can be rearranged as

$$\frac{h_t}{h} = \frac{4Wh^2}{\mu w_0^3}. \tag{21}$$

The left-hand side is recognized as a rate-of-strain for a layer of thickness h while the stress or weight per unit length is W/w_0. The factor of proportionality between them is an equivalent or Trouton viscosity

$$\mu^* = 4\mu \left(\frac{w_0}{4x}\right)^2, \tag{22}$$

where h has been replaced by the material moving interface $x(t)$. The boundary-layer thickness is seen to be of the order of the drop width w_0, a conclusion that could also be reached immediately by dimensional considerations. A composite empirical expression for the Trouton viscosity, reducing to (22) when x is small and agreeing with the two-dimensional Trouton (**19**) result $\mu_* = 4\mu$ for large x, is

$$\mu_* = 4\mu \left[1 + \frac{1}{16}\left(\frac{w_0}{x}\right)^2\right]. \tag{23}$$

This effective extensional viscosity has the necessary property that it becomes unbounded as x goes to zero, thereby enforcing the pinning of the contact points at $y = \pm w_0/2$ by solidifying the fluid there. Both the squared dependence on w_0/x and the value of the constant pre-factor $1/16$ result from the kinematical assumption that cross-sections $x =$ constant are material surfaces that remain horizontal; thus they may be modified easily if a more accurate inner model is used, and indeed there is some indication in Figs 3 and 4 that the present theory may slightly over-correct.

An entirely analogous procedure for the axisymmetric problem with base radius $w_0/2$ yields a modified Trouton viscosity

$$\mu_* = 3\mu \left[1 + \frac{1}{32}\left(\frac{w_0}{x}\right)^2\right] \tag{24}$$

for that case.

For the two-dimensional case and an initially rectangular drop of length L_0 and width w_0, the shape evolution $x = X(\xi, t)$ employing the above boundary-layer expression is the solution of a linear first-order ordinary differential equation

$$\frac{d\xi}{dx} = 1 - \frac{\rho g L_0 t}{4\mu} \frac{1 - \dfrac{\xi}{L_0}}{1 + \dfrac{w_0^2}{16x^2}} \tag{25}$$

for ξ as a function of x, and this ordinary differential equation may be integrated in closed form to yield a Lagrangian formula for the drop shape. Even without carrying out this explicit solution we can observe the Eulerian form of the solution very near the wall, where $\xi \approx x$, since then

$$y = f(x,t) = \frac{A(x,t)}{w_0 L_0} = \frac{d\xi}{dx} \approx 1 - \frac{4\rho g L_0}{\mu w_0^2} t x^2,$$

demonstrating that very near the wall, the profile is parabolic with curvature increasing linearly with time, while the actual contact points remain fixed as required.

As an example we show as the upper curves of parts (b) of Figs 3 and 4, the corrected shape of the drop with $w_0/L_0 = 0{\cdot}2$, at scaled times $t = 0{\cdot}75$ and $t = 0{\cdot}95$. These corrections were obtained by integrating equation (25) and substituting the result for $\xi = \xi(x)$ in equation (11). When compared with the (essentially exact) finite-element solution shown in parts (a) of these figures, a significantly improved agreement is clearly achieved by inclusion of this boundary-layer correction in the slender-drop theory.

6. Break points

According to the slender-drop theory for a general initial drop shape $A_0(\xi)$, the crisis time occurs when the drop's cross-section area $A(\xi, t)$ as given by equation (11) vanishes at some station ξ. Since both $A_0(\xi)$ and its integral

$$V(\xi) = \int_{\xi}^{L_0} A_0(\xi_1) d\xi_1 \tag{26}$$

(the volume lying below station ξ) are positive quantities, this must always happen at some sufficiently large time t. From equation (11), it will happen first at the station $\xi = \xi_*$ where $V(\xi)/A_0(\xi)$ takes its maximum value L_*, and then the crisis time will be

$$t_* = \frac{\mu_*}{\rho g L_*}. \tag{27}$$

The drop will then break at that station ξ_*, with the portion $0 < \xi < \xi_*$ of the original drop remaining attached to the wall, and the portion $\xi_* < \xi < L_0$ going into free fall for $t > t_*$. Whenever the crisis time is given by (27), it is convenient to refer to the quantity L_* as the 'effective length' of the drop.

The break point, effective length and crisis time, given in this simple manner by the slender-drop theory, will be correct even though we ignore the boundary-layer correction, provided only that the break point does not fall within this boundary layer, which has thickness of the same order as the drop width. Should this occur, then the breaking behaviour will vary somewhat from this prediction, as is shown by the finite-element computations.

In many cases, the quantity $V(\xi)/A_0(\xi)$ is monotone decreasing, with its maximum at the wall $\xi = 0$. Hence in such cases, the slender-drop theory predicts breakage at the wall (cf. (**21**)), with the whole initial mass going into free fall. For example, the family

$$A_0(\xi) = A_0(0)\left[1 - \frac{\xi}{L_0}\right]^n, \tag{28}$$

for any power $n > -1$, has

$$\frac{V(\xi)}{A_0(\xi)} = \frac{L_0 - \xi}{n+1}. \tag{29}$$

Hence $\xi_* = 0$ and the effective length is $L_* = L_0/(n+1)$. Note that $n = 0$ is the rectangular or cylindrical case considered earlier where the effective length is equal to the actual initial length; $n = 1$ for the axisymmetric case is a paraboloidal initial drop of a quite sensible form. Figure 5

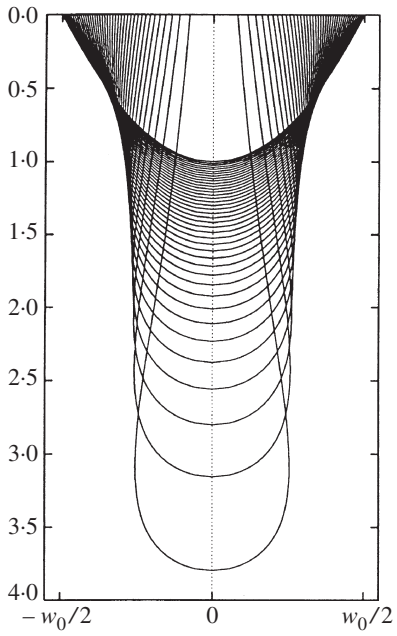

Fig. 5 Initially-paraboloidal drop ($\sigma = 0$)

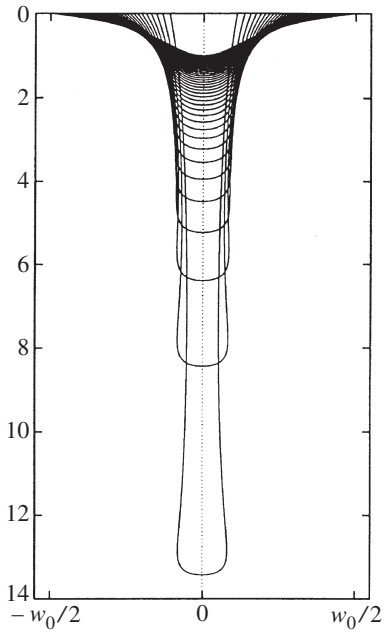

Fig. 6 Drop with $\sigma = 1{\cdot}34016$, such that half of the volume falls

shows profiles for this paraboloidal initial drop. These profiles are at a scaled time interval of 0·05, the last profile shown being at $t = 1{\cdot}95$, compared to a scaled crisis time of $t_* = 2$.

When $\xi_* = 0$, the break point is formally at the wall itself according to the slender-drop theory, and hence it lies inside the wall boundary layer. Therefore, the finite element and slender-drop solutions will differ, as we have already seen. Actual breaking occurs at a point which has an initial distance from the wall comparable with the boundary-layer thickness, with some material in that layer being left behind. However, this distance is formally of the same size as the drop width, and hence small relative to the drop length, with the volume left behind being of the order of ϵ^2, which is small compared to the total order-ϵ volume of the drop. Hence formally we can consider that the drop does indeed break at the wall as indicated by the slender-drop theory, although the actual crisis time is a little longer. Our finite-element computations confirm this description.

On the other hand, it is possible for the predicted break point to occur at a non-trivial station $\xi_* > 0$, so long as $V(\xi)/A_0(\xi)$ has an interior maximum. For example, consider an axisymmetric family of drops with initial area profiles given by

$$A_0(\xi) = A_0(0)\left(1 - \frac{\xi}{L_0}\right)\exp(Y^2 - \sigma^2), \tag{30}$$

where $Y = \sigma(1 - \xi/L_0)$ and σ is a given parameter. If $\sigma = 0$, we retrieve the paraboloidal drop

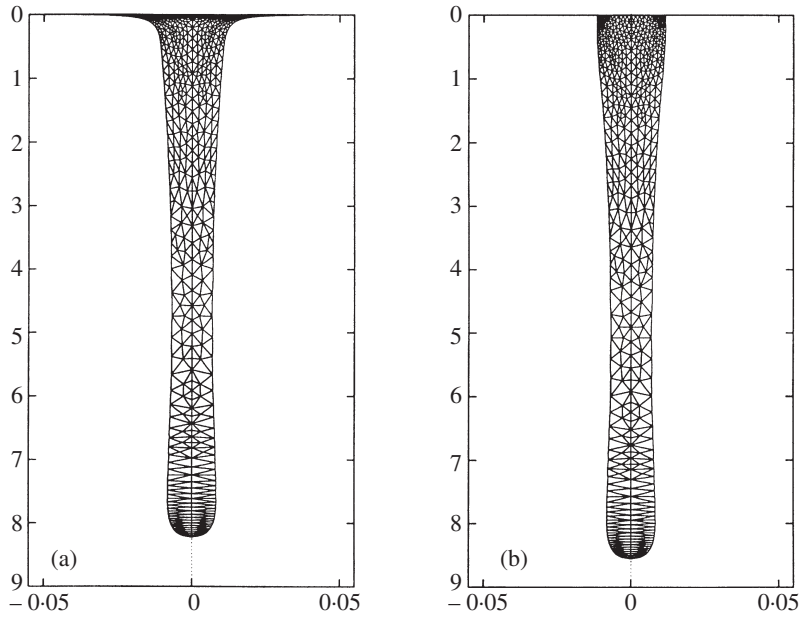

Fig. 7 Finite-element solution of drop with $\sigma = 1{\cdot}34016$ at $t = 4{\cdot}0$. (a) No-slip wall boundary, (b) slip wall boundary

$n = 1$ discussed above. We find

$$\frac{V(\xi)}{A_0(\xi)} = \left(\frac{L_0}{2\sigma}\right) \frac{1 - e^{-Y^2}}{Y}, \tag{31}$$

which has a maximum of magnitude $L_* = 0{\cdot}3191 L_0/\sigma$ at $Y = 1{\cdot}1209$. Hence if $\sigma > 1{\cdot}1209$ and the drop is sufficiently slender, breakage occurs at $\xi/L_0 = 1 - 1{\cdot}1209/\sigma$, with the above effective length L_* and hence a crisis time t_* given by (27). For example, if $\sigma = 1{\cdot}34016$, the break point $\xi/L_0 = 0{\cdot}1636$ is such that exactly half of the volume of the original drop falls, with $L_* = 0{\cdot}2381 L_0$. Figure 6 shows profiles for this case, at a scaled time interval of 0·1, the last profile shown being at a scaled time $t = 4{\cdot}1$ close to the scaled crisis time $t_* = 4{\cdot}200$. These results were computed from the slender-drop theory without allowance for the wall boundary layer, that is, with no correction for no-slip on the wall.

The same initial drop was also used as input to our finite-element code. A near-crisis profile at $t = 4{\cdot}0$ is shown in Fig.7(a), where we have taken a drop initial half-width of $0{\cdot}05 L_0$ such that the break point falls outside the boundary layer. The resemblance of the near-crisis profile to the slender-drop solution in Fig. 6 (the corresponding profile with $t = 4{\cdot}0$ being the 'next-to-end' one in that figure; note the agreement for the length $L(4{\cdot}0)/L_0 \approx 8{\cdot}3$), shows that the break point and crisis time are independent of the no-slip wall condition. To emphasize this feature, we also implemented an artificial 'slip' wall condition in our finite-element program, yielding the profile at $t = 4{\cdot}0$ shown in Fig. 7(b). The profiles for the slip and no-slip walls are remarkably similar to each other at $t = 4{\cdot}0$, and this similarity continues for times closer to the crisis time $t \approx 4{\cdot}2$.

As we increase the drop width from $0{\cdot}05 L_0$, and hence increase the vertical extent of the boundary

layer, we reach a point where the predicted break point falls within the boundary layer. When this happens, the wall boundary conditions do affect the final outcome, and the finite-element solution cannot be expected to compare as well with the slender-drop theory, for either crisis time or break point. The further the break point falls inside the boundary layer, the greater the difference between the two results. For a drop half-width of $0{\cdot}1L_0$, the break point is only just within the boundary layer, and the solution at $t = 4{\cdot}0$ is quite similar to those in Fig. 7. For times closer to crisis, however, a marked difference between a slip and no-slip wall boundary develops, showing the importance of the wall boundary condition in this case.

7. Conclusion

The emphasis in the present paper has been on the finite-time phenomenon, which was discussed by Wilson (**18**) but has not often been highlighted in the literature on extensional flows. The slender-drop approximation indicates this phenomenon explicitly for drops falling under gravity, and enables determination of crisis times, profiles and break-points in terms of simple quadratures. This theory is equivalent to one-dimensional theories of both Lagrangian and Eulerian character that have been used extensively in the literature, although the connection between the Lagrangian and Eulerian descriptions, established here, is non-trivial.

Because the wall boundary layer is not modelled by the usual slender-drop approximation, its importance is not always appreciated. We have developed a method for correcting the slender-drop theory for this boundary layer, through a modified non-constant expression for the Trouton viscosity. Nevertheless, we have demonstrated that crisis times and break points can be quite accurately predicted without this empirical correction, provided that breaking occurs below the boundary layer.

In addition, in the present paper we have used a finite-element computer program to solve the unapproximated Stokes-flow problem, both in two and three (axisymmetric) dimensions. This program was developed mainly for industrial applications, for example, in optical manufacturing, but has wide applicability for low-Reynolds number flows with free surfaces. When applied to slender drops, the finite-element program confirms the accuracy of the approximate theories. However, it is also immediately applicable to drops whose initial profile is not slender.

The example of Fig. 1 illustrates such an axisymmetric non-slender computation, where the 'honey' is initially held in a 'spoon' consisting of a shallow spherical cap. The crisis time appears in this example to correspond to an effective length of about $L_* = 0{\cdot}070R$, where R is the radius of the sphere. It is an interesting topic for further research to consider the way in which the effective length L_* depends on actual initial drop size and shape for arbitrary non-slender drops.

Acknowledgements

This work has been supported in part by the NASA Microgravity Program, by ICI, and by the Delaware Research Partnership. Support by the Australian Research Council and the Australian Postgraduate Research Awards (Industry) scheme is acknowledged.

References

1. E. O. Tuck, Mathematics of honey on toast. In *National Symposium on the Mathematical Sciences: Multiplying Australia's Potential* (ed. R. R. Moore and A. J. van der Poorten; Australian Academy of Science 1997). See also `http://www.maths.adelaide.edu.au/Applied/staff/etuck/honey_on_toast/Tuck.html`

2. J. W. White, Physical characteristics of honey. In *Honey: A Comprehensive Survey* (ed. E. Crane; Heinemann, London 1975) 207–239.
3. R. B. Bird, C. F. Curtiss, R. C. Armstrong and O. Hassager, *Dynamics of Polymeric Liquids*, 2nd edition (Wiley, New York 1987).
4. C. J. S. Petrie, *Elongational Flows* (Pitman, London 1979).
5. M. M. Denn, Continuous drawing of liquids to form fibres. *Ann. Rev. Fluid Mech.* **12** (1980) 365–387.
6. J. De Wynne, J. R. Ockendon and P. Wilmott, On a mathematical model for fiber tapering. *SIAM J. Appl. Math.* **49** (1989) 983–990.
7. P. J. Doyle, *Glass Making Today* (R.A.N. Publishers, Ohio 1994).
8. S. Rekhson, Zhong-Hao Lu and C. Day, Computer modeling of glass processing. *Coll. Papers from the 52nd Conf. on Glass Problems* Nov 12 & 13 (1991) 65–77.
9. J. E. Matta and R. P. Titus, Liquid stretching using a falling cylinder. *J. Non-Newtonian Fluid Mech.* **35** (1990) 215–229.
10. T. Sridhar, V. Tirtaatmadja, D. A. Nguyen and R. K. Gupta, Measurement of extensional viscosity of polymer solutions. *Ibid.* **40** (1991) 271–280.
11. S. Gaudet, G. H. McKinley and H. A. Stone, Extensional deformation of Newtonian liquid bridges. *Phys. Fluids* **8** (1996) 2568–2579.
12. D. Canright and S. Morris, Buoyant instability of a viscous film over a passive fluid. *J. Fluid Mech.* **255** (1993) 349–372.
13. J. Chery, A. Bonneville, J. P. Vilotte and D. Yuen, Numerical modelling of caldera dynamical behaviour. *Geophys. J. Int.* **105** (1991) 365–379.
14. G. A. Houseman and P. Molnar, Gravitational (Rayleigh–Taylor) instability of a layer with non-linear viscosity and convective thinning of continental lithosphere. *Ibid.* **128** (1997) 125–150.
15. J. Eggers, Theory of drop formation. *Phys. Fluids* **7** (1995) 941–953.
16. D. T. Papageorgiou, On the breakup of viscous liquid threads. *Ibid.* **7** (1995) 1529–1544.
17. ——, Analytical description of the breakup of liquid jets. *J. Fluid Mech.* **301** (1995) 109–132.
18. S. D. R. Wilson, The slow dripping of a viscous fluid. *Ibid.* **190** (1988) 561–570.
19. F. T. Trouton, On the coefficient of viscous traction and its relation to that of viscosity. *Proc. R. Soc.* A **77** (1906) 426–440.
20. W. W. Schultz and S. H. Davis, One-dimensional liquid fibres. *J. Rheol.* **26** (1982) 331–345.
21. A. Kaye, Convected coordinates and elongational flow. *J. Non-Newtonian Fluid Mech.* **40** (1991) 55–77.
22. P. D. Howell, Models for thin viscous sheets. *Euro. J. Appl. Math.* **7** (1996) 321–343.
23. J. T. Pittman, O. C. Zienkiewicz, R. D. Wood and J. M. Alexander, *Numerical Analysis of Forming Processes* (Wiley, New York 1984).
24. B. W. van der Fliert, P. D. Howell and J. R. Ockendon, Pressure-driven flow of a thin viscous sheet. *J. Fluid Mech.* **292** (1995) 359–376.
25. J. N. Reddy and D. K. Gartling, *The Finite Element Method in Heat Transfer and Fluid Dynamics* (CRC Press 1994).
26. R. E. Nickell, R. I. Tanner and B. Caswell, The solution of viscous incompressible jet and free-surface flows using finite-element methods. *J. Fluid Mech.* **65** (1974) 189–206.
27. R. W. G. Shipman, M. M. Denn and R. Keunings, Mechanics of the 'falling plate' extensional rheometer. *J. Non-Newtonian Fluid Mech.* **40** (1991) 281–288.
28. D. M. Burley and S. J. Graham, The blowing of thin films into moulds with applications in the glass container industry. *The Mathematics of Finite Elements and Applications* **7** (1991)

279–286.

29. S. J. Graham, D. M. Burley and J. C. Carling, Fluid flow in thin films using finite elements. *Math. Engng Ind.* **3** (1992) 229–246.

30. J. H. Williams, D. R. J. Owen and J. M. A. C. Sa, The numerical modelling of glass forming processes. *Collected papers, 14th Intl. Congr. on Glass* (1986) 138–145.

31. E. O. Tuck, Y. M. Stokes and L. W. Schwartz, Slow slumping of a very viscous liquid bridge. *J. Engng Math.* **32** (1997) 31–44.

32. Y. M. Stokes, Creeping-flow computational modelling of optical quality free surfaces formed by slumping of molten glass. In *Computational Techniques and Applications: CTAC97* (ed. B. J. Noye, M. D. Teubner and A. W. Gill; World Scientific, Singapore 1998) 671–678.

33. Y. M. Stokes, Very viscous flows driven by gravity, with particular application to slumping of molten glass. Ph.D. Thesis, The University of Adelaide (1998).

34. G. K. Batchelor, *An Introduction to Fluid Dynamics* (Cambridge, London 1967).

35. J. V. Wehausen and E. V. Laitone, Surface Waves. In *Handbuch der Physik*, Vol. 9 (ed. S. Flugge; Springer, Berlin 1960) 446–778.

36. O. C. Zienkiewicz and R. L. Taylor, *The Finite Element Method*, 4th edition, Vol. 1 (McGraw–Hill, New York 1989).

37. A. Cameron, *The Principles of Lubrication* (Longmans, London 1966).